PHYSICAL REVIEW B **96**, 041126(R) (2017)

Emergent Weyl nodes and Fermi arcs in a Floquet Weyl semimetal

Leda Bucciantini,[1,2] Sthitadhi Roy,[1] Sota Kitamura,[3] and Takashi Oka[1,2]
[1]*Max-Planck-Institut für Physik komplexer Systeme, Nöthnitzer Straße 38, 01187 Dresden, Germany*
[2]*Max-Planck-Institut für Chemische Physik fester Stoffe, Nöthnitzer Straße 40, 01187 Dresden, Germany*
[3]*Department of Physics, University of Tokyo, Hongo, Tokyo 113-0033, Japan*
(Received 13 December 2016; revised manuscript received 25 March 2017; published 27 July 2017)

When a Dirac semimetal is subject to a circularly polarized laser, it is predicted that the Dirac cone splits into two Weyl nodes and a nonequilibrium transient state called the Floquet Weyl semimetal is realized. We focus on the previously unexplored low-frequency regime, where the upper and lower Dirac bands resonantly couple with each other through multiphoton processes, which is a realistic situation in solid-state ultrafast pump-probe experiments. We find a series of new Weyl nodes emerging in pairs when the Floquet replica bands hybridize with each other. The nature of the Floquet Weyl semimetal with regard to the number, locations, and monopole charges of these Weyl nodes is highly tunable with the amplitude and frequency of the light. We derive an effective low-energy theory using Brillouin-Wigner expansion and further regularize the theory on a cubic lattice. The monopole charges obtained from the low-energy Hamiltonian can be reconciled with the number of Fermi arcs on the lattice, which we find numerically.

DOI: 10.1103/PhysRevB.96.041126

Introduction. Weyl semimetals (WSM) and Dirac semimetals (DSM) have emerged as one of the most exciting new class of three-dimensional topological materials [1–6] with a gapless and linearly dispersing bulk spectrum allowing for a realization of Weyl fermions. Since the Weyl nodes in a lattice always occur in pairs of opposite chiralities [7], they act as monopoles and antimonopoles of Berry flux. Consequently, WSMs have topological surface states whose Fermi surfaces originate and terminate at Weyl nodes of opposite chiralities leading to open Fermi arcs [8–15]. The nontrivial topology of WSMs leads to various exotic electromagnetic responses like the condensed matter realization of the chiral anomaly [16–22], chiral magnetic effect [23,24], and negative magnetoresistance [19,25,26]. Although WSM materials have been discovered recently [13–15,27–29], it is extremely desirable to posses the capability of tuning their properties with regard to the number and nature of Weyl nodes. It is known that WSM can be generated out of a DSM when time-reversal (TRS) and/or inversion symmetries are broken [2,30–32]. While the former separates the Weyl nodes in momentum, the latter separates them in energy.

Recently, time periodic modulations of topologically trivial systems, often realized via light-matter interaction, have emerged as an interesting way of obtaining topological phases, often richer than their static counterparts [33–45]; the effects of interaction and disorder have also been explored [46–51]. Such protocols have also been complemented with their experimental realizations [52,53].

In the same spirit, one expects to generate a three-dimensional topological WSM from its trivial parent, a Dirac semimetal (DSM) by subjecting it to time-periodic fields [54–59]. An appealing way of breaking TRS in the context of solid state experiments is to subject DSM materials like Na_3Bi and Cd_3As_2 [60–64] to a circularly polarized laser (CPL). Such a system is described by a Hamiltonian periodic in time and hence can be studied using Floquet theory [65–67]. Analysis of the Floquet quasienergy spectrum reveals a new Floquet WSM phase born out of the DSM, in which the number, location, and nature of the Weyl nodes are tunable with the amplitude and frequency of CPL. Previously, such a system has been studied within the framework of high-frequency Floquet-Magnus expansion [68,69] and holographic duality [70].

The focus of this work, however, is the much richer and experimentally relevant regime, namely the situation where the frequency of the CPL is much less than or comparable to the bandwidth of the parent DSM. In this regime, Floquet replica, i.e., photon dressed states, will cross, hybridize with and repel each other. As a consequence, besides the two Weyl nodes born out of the original Dirac cone, we find a series of infinite number of Weyl nodes emerging from the Floquet replicas. They have nontrivial monopole charges, and as the CPL amplitude is increased, they move and pairwise annihilate as they approach those with opposite monopole numbers (see Fig. 1, for example).

We derive effective low-energy Hamiltonians for these new Weyl nodes using Brillouin-Wigner expansion [71–73] and deduce their monopole charges. Similar to the static case, Floquet Fermi arcs are generated between the Weyl nodes and their degeneracy is related to the monopole number of the Weyl nodes. These results are verified by regularizing our theory on a lattice, and numerically computing the number of Fermi arcs in a system with open boundaries. Our findings can be experimentally realized using time-resolved ARPES or ultrafast pump-probe measurements, which we will explain in the end.

Spectrum of the Floquet WSM. Floquet theory reduces the solution of the Schrödinger equation for a time periodic Hamiltonian $\mathcal{H}(t+T)=\mathcal{H}(t)$ with $T=2\pi/\Omega$ to an eigenvalue problem for a time-independent, but infinite dimensional, Hamiltonian (for a review see [74]). The infinite dimensional Floquet Hamiltonian $\mathcal{H}^F$ has blocks of the general form

$$\mathcal{H}^F_{m,n}=\frac{1}{T}\int_{-T/2}^{T/2}dt e^{i(m-n)\Omega t}\mathcal{H}(t)-n\Omega\delta_{m,n}, \qquad (1)$$

where $n,m\in\mathbb{Z}$. The diagonal block $\mathcal{H}^F_{n,n}$ corresponding to the n-photon sector is equal to the time averaged Hamiltonian over

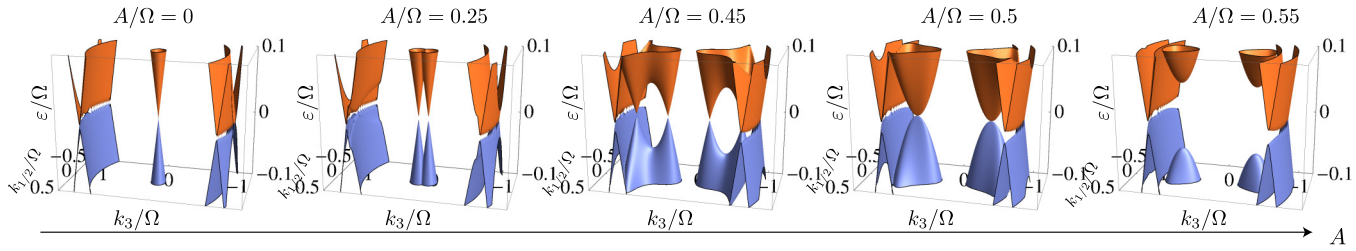

FIG. 1. Evolution of the Floquet quasienergy spectrum on increasing laser amplitude A. Weyl points generated from the $n = 0$ and $n = \pm 1$ sectors at finite A meet and annihilate at $A/\Omega = 0.5$.

a period $\mathcal{H}_0^F$, shifted in energy by $n\Omega$. The off-diagonal blocks $\mathcal{H}_{m,n}^F = \mathcal{H}_{m-n}^F$, with $m \neq n$, correspond to transitions between these sectors via absorption or emission of $m - n$ photons.

We start with a continuum low-energy description of the DSM described by the Hamiltonian $\mathcal{H}_{\rm DSM} = \gamma^0(Mc^2 + c\hbar\boldsymbol{\gamma}\cdot\mathbf{k})$, where M is the mass and c the Fermi velocity of the DSM. The CPL propagating along the $\hat{z}$, described by the gauge field $\mathbf{A}(\mathbf{r},t)$, is assumed to have a wavelength much larger than the width of the DSM along $\hat{z}$. Further, since the magnetic field of the CPL is negligible compared to the electric field, the $\mathbf{r}$ dependence can be neglected, which reduces the form of the gauge field to $\mathbf{A}(t) = A\{\cos(\Omega t), \sin(\Omega t), 0\}$, where $E = A\Omega$ is the amplitude of the electric field and Ω is the frequency of the CPL. The continuum time-dependent Hamiltonian describing the DSM subjected to CPL can then be obtained via minimal coupling between $\mathcal{H}_{\rm DSM}$ and $\mathbf{A}(t)$ as

$$\mathcal{H}(t) = \gamma^0\Big[Mc^2 + \hbar c\boldsymbol{\gamma}\cdot\Big(\mathbf{k} - \frac{e}{\hbar}\mathbf{A}(t)\Big)\Big]. \tag{2}$$

In the following, we use natural units with $\hbar = 1 = e = c$ and also set the mass M of the DSM to zero. The Floquet Hamiltonian corresponding to $\mathcal{H}(t)$ (2) can be obtained using Eq. (1) as

$$\mathcal{H}_0^F = \gamma^0\boldsymbol{\gamma}\cdot\mathbf{k};\ \mathcal{H}_{\pm 1}^F = -A\gamma^0\gamma^{\pm}, \tag{3}$$

and $\mathcal{H}_n^F = 0 \forall |n| > 1$, where $\gamma^{\pm} = (\gamma^1 \pm \imath\gamma^2)/2$. To obtain the Floquet quasienergy spectrum, i.e., the eigenvalues ε of the Floquet Hamiltonian, $\mathcal{H}^F$ is truncated to include a finite number of photon processes and numerically diagonalized. Since we are interested in the low-energy properties of the system, it is sufficient to include up to ± 5 photon sectors, so that the Floquet quasienergy spectrum within $\pm 3\Omega$ converges to numerical precision.

The quasienergy spectrum reveals an exotic Floquet WSM phase, where the number and locations of the Weyl nodes can be tuned via A and Ω as shown in Fig. 1. In the absence of CPL ($A = 0$), the Floquet quasienergy spectrum consists of a doubly degenerate Dirac cone at $\mathbf{k} = 0$ and quasienergy $\varepsilon = 0$. Additionally, the gap between the Floquet replicas of the spectrum from the $\pm n$-photon sectors closes on the hypersphere $|\mathbf{k}| = n\Omega$ at $\varepsilon = 0$. A finite A causes the Dirac cones at $\mathbf{k} = 0$ to hybridize with each other, and similarly the doubly-degenerate gapless hyperspheres at $|\mathbf{k}| = n\Omega$. Each of these split into two Weyl nodes, lying on the k_3 axis. On increasing A, the Weyl nodes move along k_3, such that they eventually merge and annihilate each other, resulting in a gapped spectrum. The global picture is shown in Figs. 2(a) and 2(b) via the trajectories of the Weyl nodes.

It is important to note that, although the continuum theory is scale-invariant because of its linear dispersion, leading to any Ω being resonant, it correctly describes the physics of a lattice regularized theory only close to $\mathbf{k} = 0$ within the region where the linear approximation for the DSM spectrum $\sin|\mathbf{k}| \sim |\mathbf{k}|$ holds. The spectrum of a DSM on a lattice would have a bounded spectrum with a finite bandwidth. The resonant regime in this case, unlike the high-frequency limit, allows for hybridization between the $n = \pm 1$ Floquet replicas [75] resulting in additional Weyl nodes as shown for small Ω/Ω_0 values in Fig. 2(b). It can be estimated that the continuum theory correctly captures the resonances between $\pm n$-photon sectors as long as Ω is small enough such that $\sin(n\Omega) \sim n\Omega$. Having established that the resonant limit of the Floquet WSM indeed leads to new Weyl nodes from resonances between higher photon sectors, we now obtain effective low-energy

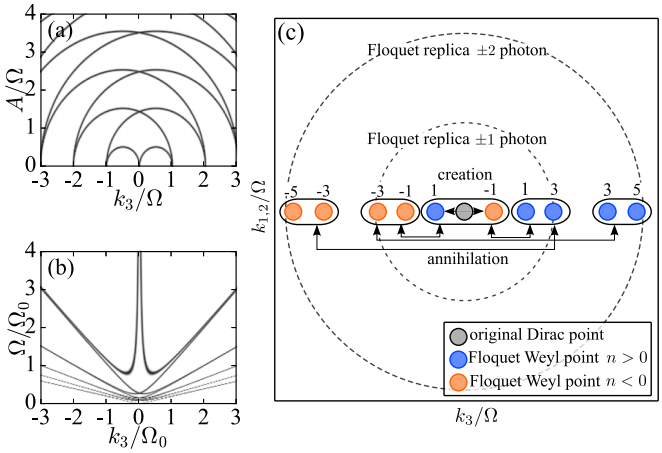

FIG. 2. The number and location of Weyl points along k_3 calculated from the continuum model as a function of (a) the amplitude A and (b) frequency Ω of the circularly polarized light, with $A = \Omega_0/4$ fixed, where Ω_0 is an arbitrarily chosen frequency. The lines denote the location of the Weyl points on the k_3 axis, which are calculated by locating the zeros of the quasienergy spectrum. Note that, on decreasing Ω, the spectrum has increasing number of Weyl points close to $k_3 = 0$ originating from higher order resonances. (c) Schematic plot showing the creation and annihilation of emergent Weyl nodes along the k_z axis, when $A \neq 0$. The dashed circles show the Dirac semimetal nodal line due to Floquet replica bands crossing the $\varepsilon = 0$ surface at $|\mathbf{k}| = n\Omega$, for $A = 0$, $\Omega \neq 0$, which disappears as soon as the CPL is turned on. The number above each Weyl point indicates its monopole charge, which is computed from the effective Hamiltonian in Eq. (5).

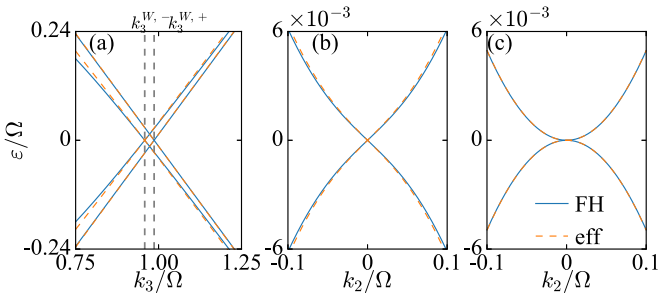

FIG. 3. Floquet quasienergy spectrum near the Weyl nodes for $A = \Omega/5$. The spectrum from the Floquet Hamiltonian (FH) (3) and effective theory obtained from (5) are compared. (a) A slice along k_3 with $k_{1,2} = 0$. A slice along k_2 for (b) $k_3 = k_3^{W,+}$ and (c) $k_3 = k_3^{W,-}$ at $k_1 = 0$.

Hamiltonians for these new Weyl nodes originating from the hybridization of $n = \pm 1$ Floquet replicas, i.e., near $k_3 \simeq \pm\Omega$, to leading order in A.

Effective theory for the emergent Weyl nodes. The Weyl nodes that are created in the Floquet replica bands have nontrivial monopole numbers and we can construct their

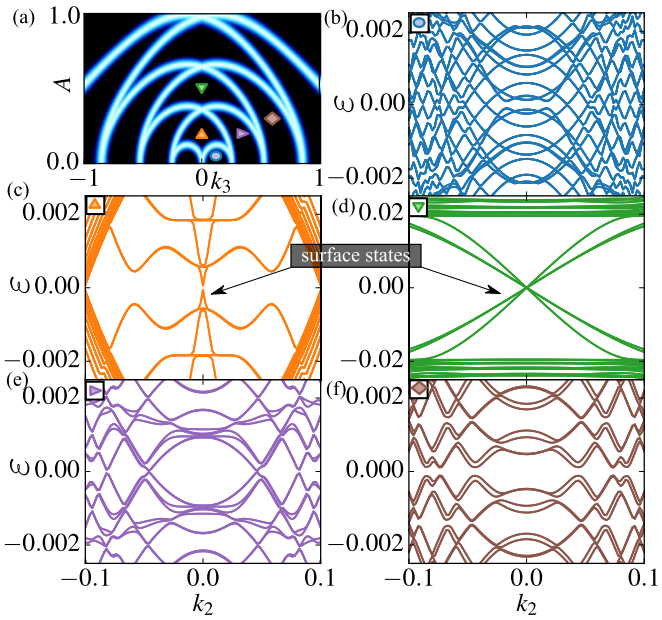

FIG. 4. (a) Weyl node trajectories similar to Fig. 1 for the lattice system with $\Omega = 0.25$. The markers in the plot correspond to the values of A and k_3 for which the quasienergy spectrum with open boundary conditions is shown. In plots (b), (e), and (f), there are no surface states; in (c) and (d) there are respectively one and three surface states. From the change in the number of Fermi arcs between the regions marked by the blue circle and the orange and purple triangles, it can be deduced that the monopole charges of the Weyl nodes from the $n = \pm 1$ sectors are 1 and -1, respectively. Similarly, from the regions marked with the green and purple triangles and the brown diamond, it can be deduced that the monopole charges of the Weyl nodes $n = \pm 2$ sectors are ± 3. Note that, each of the Fermi arcs shown here are twofold degenerate due to equivalent contributions from $k_1 = 0$ and π. The system has a linear dimension of 512 and $\mathcal{H}^F$ is truncated till $n = 4$.

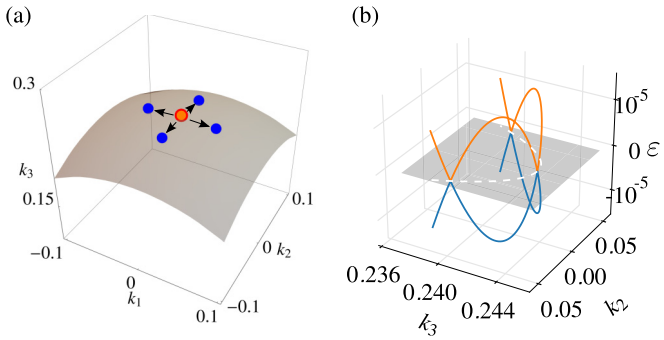

FIG. 5. Splitting of Weyl points due to $C-4$ symmetric lattice. (a) The original Weyl point obtained from the continuum theory with monopole charge of $+3$ (red) is split into four $C-4$ symmetric Weyl points (blue) with charges of $+1$ each while the monopole charge of the original Weyl point on the k_3 axis now becomes -1 (orange). (b) The quasienergy bands along the white dashed line are shown, which corresponds to the minima of the quasienergy spectrum in the k_2-k_3 plane for $k_1 = 0$ illustrating the additional Weyl points apart from the one at $k_2 = 0$. The parameters used are $\Omega = 0.25$ and $A = 0.08$.

effective theories using the Brillouin-Wigner (BW) expansion, where the details can be found in Ref. [76]. We note that this method is equivalent to the Green's function decimation (GFD) technique [77,78], which has also been applied to study Floquet states in graphene [75].

Here, we demonstrate this for the first Weyl node pairs created by hybridization of the $n = \pm 1$ Floquet replicas that are resonant at $k_3 \simeq \Omega$ and $k_{1,2} = 0$. The derivation is done by projecting the infinite-dimensional Floquet Hamiltonian (3) onto the relevant photon sectors that participate in the resonance. Their effective coupling is derived up to leading orders in A by projecting out other photon sectors. Given the eigenvalue problem $\sum_n (\mathcal{H}^F_{m,n} - \delta_{m,n} m\Omega)|\Psi_n\rangle = \varepsilon|\Psi_m\rangle$, we aim to reduce it to an eigenvalue problem $\sum_n{}' \mathcal{H}^{\rm BW}_{m,n} P|\Psi_n\rangle = \varepsilon P|\Psi_m\rangle$ in a smaller Hilbert space. P is the projection operator to the $n = \pm 1$ subspace, $P_{m,n} = \delta_{m,1}\delta_{n,1} + \delta_{m,-1}\delta_{n,-1}$ and the sum $\sum'$ is restricted to this space. The BW Hamiltonian depends on the exact eigenvalue ε and up to A^2 it is expressed as

$$\begin{aligned}\mathcal{H}^{\rm BW}_{s,s}(\varepsilon) &= \mathcal{H}^F_0 - s\Omega + \mathcal{H}^F_{+s}\left(\varepsilon - \mathcal{H}^F_0\right)^{-1}\mathcal{H}^F_{-s} \\ &\quad + \mathcal{H}^F_{-s}\left(\varepsilon + 2s\Omega - \mathcal{H}^F_0\right)^{-1}\mathcal{H}^F_{-s}; \\ \mathcal{H}^{\rm BW}_{s,-s}(\varepsilon) &= \mathcal{H}^F_{+s}\left(\varepsilon - \mathcal{H}^F_0\right)^{-1}\mathcal{H}^F_{+s}, \end{aligned} \tag{4}$$

with $s = \pm 1$. By using the basis diagonal in both $\mathcal{H}^F_0$ and γ^5, one can further project out the irrelevant states far from $\varepsilon = 0$, and replace ε with an explicit form obtained by an expansion in A. The effective Hamiltonian so obtained has the same block diagonal structure as obtained from GFD and the two blocks are given by

$$\begin{aligned}\mathcal{H}^{W,\pm}_{\rm eff} &= \left(|\mathbf{k}| - \Omega + A^2\frac{|\mathbf{k}|^2 + k_3^2 \pm \Omega k_3}{|\mathbf{k}|(4|\mathbf{k}|^2 - \Omega^2)}\right)\sigma^3 \\ &\quad - \frac{A^2\left(|\mathbf{k}| + k_3\right)^{\pm 1}}{2|\mathbf{k}|\Omega(2|\mathbf{k}| - \Omega)}\left(k_+^{2\mp 1}\sigma^+ + \text{H.c.}\right), \end{aligned} \tag{5}$$

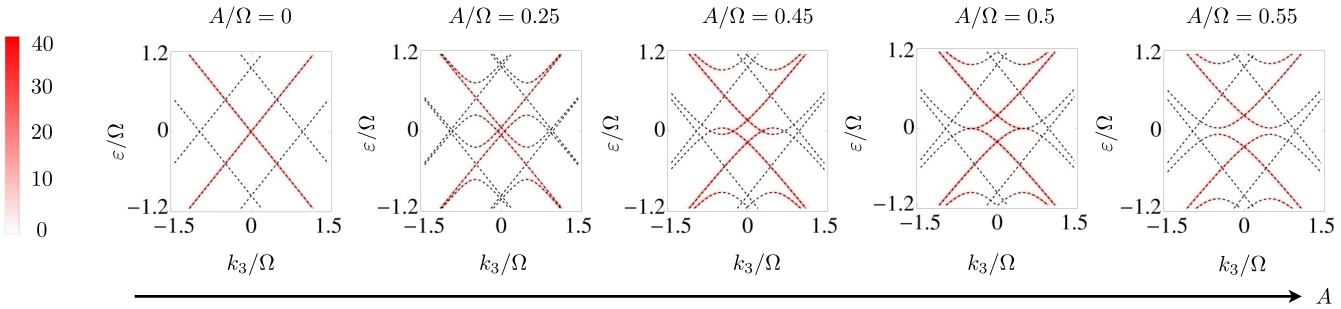

FIG. 6. Evolution of the population of the Floquet quasienergy bands as a function of A/Ω, when starting from an initial state that has the two upper and lower Dirac bands fully occupied. Dashed lines indicate the Floquet quasienergy bands, while the red shade indicate the bands, which have larger spectral weight.

where $k_\pm = k_1 \pm ik_2$ and $\sigma_\pm = \frac{\sigma_1 \pm i\sigma_2}{2}$. The Weyl points appear at

$$k_3^{W,\pm} = \frac{(2 \mp 1)\Omega + \sqrt{((2 \pm 1)\Omega)^2 - 8A^2}}{4}, \quad k_{1,2} = 0, \tag{6}$$

which agree with the numerical results as shown in Fig. 3. Equation (5) further implies that the monopole charges are $+1$ and $+3$. One can generalize this discussion to $k_3 \sim n\Omega$ with $\pm n$-photon sectors, where the off diagonal term is proportional to $A^n(k_+^{2n\mp1}\sigma^+ + \text{h.c.})$ to leading orders in A implying monopole numbers of $2n \mp 1$. In the negative $k_3 < 0$ side, we obtain Weyl nodes with $-2n \pm 1$ monopole numbers, and the pair annihilation shown in Fig. 2 occurs between those with opposite monopole numbers. We note that similar nodal states with nontrivial winding were studied in the two-dimensional problem as well [79].

Emergent Fermi arcs and lattice effects. In a system with open boundary conditions, the monopole charge of the Weyl nodes can then be deduced from the change in the number and chirality of the Fermi arcs edge states across the Weyl nodes. Equivalently, a WSM can be viewed as a momentum-space stack (along k_3 in this case) of two-dimensional Chern insulators with a k_3 dependent mass, where the Weyl nodes serve as points of topological phase transitions leading to a change in the Chern number and hence in the number of edge states. In order to reconcile the number of edge states with the monopole charges of the Floquet Weyl nodes, we regularize our continuum theory on a four-orbital cubic lattice and study the quasienergy spectrum of with open boundary conditions along x but periodic along y and z.

Here, using a four-orbital fermion operator $\Psi_{\hat{\mu}}$, we consider a lattice model

$$\mathcal{H}(t) = -\frac{1}{2}\sum_{\mathbf{r}}\sum_{\mu=1}^{3}(\iota\Psi_{\mathbf{r}}^\dagger\gamma^0\gamma^\mu\Psi_{\mathbf{r}+\hat{\mu}}e^{-\iota\mathbf{A}(t)\cdot\hat{\mu}} + \text{H.c.}) \tag{7}$$

as a regularized version of the DSM in CPL incorporated as a time-dependent Peierl's substitution. In momentum space, it reduces to $\mathcal{H}_{\text{DSM}} = -\sum_{\mu=1}^{3}\gamma^0\gamma^\mu\sin(k_\mu - A_\mu)$. Using Eq. (1), the components of the Floquet Hamiltonian for the lattice system become

$$\begin{aligned}\mathcal{H}_m^F &= -\tfrac{1}{2}J_m(A)[(-\iota)^m\lambda_1 + (-\iota)^{-m}\lambda_1^\dagger + \lambda_2 + (-1)^m\lambda_2^\dagger] \\ \mathcal{H}_0^F &= -\tfrac{1}{2}[J_0(A)(\lambda_1 + \lambda_2) + \lambda_3] + \text{H.c.},\end{aligned} \tag{8}$$

where $\lambda_\mu = \iota\sum_{\mathbf{r}}\Psi_{\mathbf{r}}^\dagger\gamma^0\gamma^\mu\Psi_{\mathbf{r}+\hat{\mu}}$ and J_m is the m^{th} Bessel function of the first kind.

The lattice Hamiltonian allows direct transitions between all photon sectors and may result in a difference in the monopole charge of Weyl nodes compared with the continuum theory. For instance, $\mathcal{H}_{\pm2}^F$ give an additional off-diagonal term $\sim -(A^2/8)k_-\sigma^+ + \text{H.c.}$ to $\mathcal{H}_{\text{eff}}^{W,-}$ in Eq. (5). This term changes the monopole charge from $+3$ to -1 in the vicinity of $k_3 = k_3^{W,-}$. This is manifested in the number of the Fermi arcs changing by one across this Weyl point as shown in the regions corresponding to the blue circle and the orange and purple triangles in Fig 4. Regularizing the theory on a $C-4$ symmetric lattice essentially leads to four additional Weyl points with charges $+1$ branching out away from the k_3 axis such that their net charges and that of the one on the k_3 axis sum to -3, which is shown in Fig. 5. A simple counting of edge states in Fig. 4 also shows that that the monopole charges of the Weyl nodes generated from the $n = \pm2$-photon sector are ±3.

Tr-ARPES is a powerful method to experimentally observe the Floquet bands. The static spectral function gives a reliable approximation if the bands are initially fully occupied and the laser is turned on suddenly. It is defined by $A(k,\varepsilon) = -\pi^{-1}\text{Tr}[(\varepsilon + i\delta)I - \mathcal{H}_k^F]^{-1}$, where $\mathcal{H}^F$ is the Floquet Hamiltonian, Tr denotes the trace over Floquet and internal states, and δ is a small real number, see Ref. [33] for details. As shown in Fig. 6, where we considered an initial state with the four original Dirac bands fully occupied, most of the spectral weight is concentrated near the original Dirac bands even for $A/\Omega \neq 0$; in particular, the annihilation process at $A/\Omega = 0.5$ has enough spectral weight to be experimentally observable.

Conclusions. To summarize, we have derived an effective low-energy theory for a Floquet WSM obtained by subjecting a DSM to CPL. We especially focused on the Weyl points originating from the Floquet replica in the resonant limit. We found that tuning the frequency or the amplitude of the CPL can move these Weyl points such that they can merge and annihilate in pairs. We also found that such a Floquet WSM allows for Weyl points of higher monopole charges, which we finally reconciled by numerically studying the number of Fermi arcs on a lattice system.

The annihilation process of Weyl nodes is experimentally accessible. The Fermi velocity of the DSM Cd_3As_2 is $1.5 \times 10^6\ \text{m s}^{-1}$ [63]. If a mid infrared laser with photon energy $\Omega = 0.2$ eV is used, the pair annihilation taking place at $A/\Omega = 0.5$

can be achieved at $E \simeq 0.2$ MeV cm^{-1}. Our results can potentially be verified using time-resolved ARPES, as it has already been successfully performed in Refs. [52,53] to obtain the Floquet replicas in Bi_2Se_3.

Acknowledgments. This work is partially supported by KAKENHI (Grant No. 23740260) and from the ImPact project (No. 2015-PM12-05-01) from Japan Science and Technology Agency (JST).

[1] S. Murakami, Phase transition between the quantum spin Hall and insulator phases in 3D: emergence of a topological gapless phase, New J. Phys. **9**, 356 (2007).

[2] A. A. Burkov and L. Balents, Weyl Semimetal in a Topological Insulator Multilayer, Phys. Rev. Lett. **107**, 127205 (2011).

[3] P. Hosur and X. Qi, Recent developments in transport phenomena in Weyl semimetals, C. R. Phys. **14**, 857 (2013).

[4] A. M. Turner and A. Vishwanath, Beyond Band Insulators: Topology of Semi-metals and Interacting Phases, arXiv:1301.0330.

[5] O. Vafek and A. Vishwanath, Dirac Fermions in Solids: From High-T_c Cuprates and Graphene to Topological Insulators and Weyl Semimetals, Annu. Rev. Condens. Matter Phys. **5**, 83 (2014).

[6] S. Jia, S.-Y. Xu, and M. Z. Hasan, Weyl semimetals, fermi arcs and chiral anomalies, Nat. Mater. **15**, 1140 (2016).

[7] H. B. Nielsen and M. Ninomiya, A no-go theorem for regularizing chiral fermions, Phys. Lett. B **105**, 219 (1981).

[8] X. Wan, A. M. Turner, A. Vishwanath, and S. Y. Savrasov, Topological semimetal and Fermi-arc surface states in the electronic structure of pyrochlore iridates, Phys. Rev. B **83**, 205101 (2011).

[9] P. Hosur, Friedel oscillations due to Fermi arcs in Weyl semimetals, Phys. Rev. B **86**, 195102 (2012).

[10] T. Ojanen, Helical Fermi arcs and surface states in time-reversal invariant Weyl semimetals, Phys. Rev. B **87**, 245112 (2013).

[11] R. Okugawa and S. Murakami, Dispersion of Fermi arcs in Weyl semimetals and their evolutions to Dirac cones, Phys. Rev. B **89**, 235315 (2014).

[12] A. C. Potter, I. Kimchi, and A. Vishwanath, Quantum oscillations from surface Fermi arcs in Weyl and Dirac semimetals, Nat. Commun. **5**, 5161 (2014).

[13] S.-Y. Xu, I. Belopolski, N. Alidoust, M. Neupane, G. Bian, C. Zhang, R. Sankar, G. Chang, Z. Yuan, C.-C. Lee, S.-M. Huang, H. Zheng, J. Ma, D. S. Sanchez, B. Wang, A. Bansil, F. Chou, P. P. Shibayev, H. Lin, S. Jia, and M. Z. Hasan, Discovery of a weyl fermion semimetal and topological fermi arcs, Science **349**, 613 (2015).

[14] S.-Y. Xu, N. Alidoust, I. Belopolski, Z. Yuan, G. Bian, T.-R. Chang, H. Zheng, V. N. Strocov, D. S. Sanchez, G. Chang, C. Zhang, D. Mou, Y. Wu, L. Huang, C.-C. Lee, S.-M. Huang, B. Wang, A. Bansil, H.-T. Jeng, T. Neupert, A. Kaminski, H. Lin, S. Jia, and M. Z. Hasan, Discovery of a Weyl fermion state with fermi arcs in niobium arsenide, Nat. Phys. **11**, 748 (2015).

[15] S.-M. Huang, S.-Y. Xu, I. Belopolski, C.-C. Lee, G. Chang, B. Wang, N. Alidoust, G. Bian, M. Neupane, C. Zhang, S. Jia, A. Bansil, H. Lin, and M. Z. Hasan, A Weyl Fermion semimetal with surface Fermi arcs in the transition metal monopnictide TaAs class, Nat. Commun. **6**, 7373 (2015).

[16] H. B. Nielsen and M. Ninomiya, The Adler-Bell-Jackiw anomaly and Weyl fermions in a crystal, Phys. Lett. B. **130**, 389 (1983).

[17] A. G. Grushin, Consequences of a condensed matter realization of lorentz-violating qed in weyl semi-metals, Phys. Rev. D **86**, 045001 (2012).

[18] A. A. Zyuzin and A. A. Burkov, Topological response in Weyl semimetals and the chiral anomaly, Phys. Rev. B **86**, 115133 (2012).

[19] D. T. Son and B. Z. Spivak, Chiral anomaly and classical negative magnetoresistance of weyl metals, Phys. Rev. B **88**, 104412 (2013).

[20] K. Landsteiner, Anomalous transport of Weyl fermions in Weyl semimetals, Phys. Rev. B **89**, 075124 (2014).

[21] J. Behrends, A. G. Grushin, T. Ojanen, and J. H. Bardarson, Visualizing the chiral anomaly in Dirac and Weyl semimetals with photoemission spectroscopy, Phys. Rev. B **93**, 075114 (2016).

[22] S. Roy, M. Kolodrubetz, J. E. Moore, and A. G. Grushin, Chern numbers and chiral anomalies in Weyl butterflies, Phys. Rev. B **94**, 161107(R) (2016).

[23] K. Fukushima, D. E. Kharzeev, and H. J. Warringa, Chiral magnetic effect, Phys. Rev. D **78**, 074033 (2008).

[24] D. T. Son and N. Yamamoto, Berry Curvature, Triangle Anomalies, and the Chiral Magnetic Effect in Fermi Liquids, Phys. Rev. Lett. **109**, 181602 (2012).

[25] A. A. Burkov, Negative longitudinal magnetoresistance in Dirac and Weyl metals, Phys. Rev. B **91**, 245157 (2015).

[26] F. Arnold, C. Shekhar, S.-C. Wu, Y. Sun, R. D. Dos Reis, N. Kumar, M. Naumann, M. O. Ajeesh, M. Schmidt, A. G. Grushin, J. H. Bardarson, M. Baenitz, D. Sokolov, H. Borrmann, M. Nicklas, C. Felser, E. Hassinger, and B. Yan, Negative magnetoresistance without well-defined chirality in the Weyl semimetal TaP, Nat. Commun. **7**, 11615 (2016).

[27] B. Q. Lv, H. M. Weng, B. B. Fu, X. P. Wang, H. Miao, J. Ma, P. Richard, X. C. Huang, L. X. Zhao, G. F. Chen, Z. Fang, X. Dai, T. Qian, and H. Ding, Experimental Discovery of Weyl Semimetal TaAs, Phys. Rev. X **5**, 031013 (2015).

[28] B. Q. Lv, N. Xu, H. M. Weng, J. Z. Ma, P. Richard, X. C. Huang, L. X. Zhao, G. F. Chen, C. E. Matt, F. Bisti, V. N. Strocov, J. Mesot, Z. Fang, X. Dai, T. Qian, M. Shi, and H. Ding, Observation of Weyl nodes in TaAs, Nat. Phys. **11**, 724 (2015).

[29] L. X. Yang, Z. K. Liu, Y. Sun, H. Peng, H. F. Yang, T. Zhang, B. Zhou, Y. Zhang, Y. F. Guo, M. Rahn, D. Prabhakaran, Z. Hussain, S. K. Mo, C. Felser, B. Yan, and Y. L. Chen, Weyl semimetal phase in the non-centrosymmetric compound taas, Nat. Phys. **11**, 728 (2015).

[30] A. A. Zyuzin, S. Wu, and A. A. Burkov, Weyl semimetal with broken time reversal and inversion symmetries, Phys. Rev. B **85**, 165110 (2012).

[31] G. Halász and L. Balents, Time-reversal invariant realization of the weyl semimetal phase, Phys. Rev. B **85**, 035103 (2012).

[32] H. Weng, C. Fang, Z. Fang, B. A. Bernevig, and X. Dai, Weyl Semimetal Phase in Noncentrosymmetric Transition-Metal Monophosphides, Phys. Rev. X **5**, 011029 (2015).

[33] T. Oka and H. Aoki, Photovoltaic hall effect in graphene, Phys. Rev. B **79**, 081406 (2009).

[34] J.-i. Inoue and A. Tanaka, Photoinduced Transition Between Conventional and Topological Insulators in Two-Dimensional Electronic Systems, Phys. Rev. Lett. **105**, 017401 (2010).

[35] N. H. Lindner, G. Refael, and V. Galitski, Floquet topological insulator in semiconductor quantum wells, Nat. Phys. **7**, 490 (2011).

[36] Z. Gu, H. A. Fertig, D. P. Arovas, and A. Auerbach, Floquet Spectrum and Transport Through an Irradiated Graphene Ribbon, Phys. Rev. Lett. **107**, 216601 (2011).

[37] T. Kitagawa, T. Oka, A. Brataas, L. Fu, and E. Demler, Transport properties of nonequilibrium systems under the application of light: Photoinduced quantum hall insulators without landau levels, Phys. Rev. B **84**, 235108 (2011).

[38] N. H. Lindner, D. L. Bergman, G. Refael, and V. Galitski, Topological floquet spectrum in three dimensions via a two-photon resonance, Phys. Rev. B **87**, 235131 (2013).

[39] J. Cayssol, B. Dóra, F. Simon, and R. Moessner, Floquet topological insulators, Phys. Status Solidi (RRL) **7**, 101 (2013).

[40] P. Delplace, Á. Gómez-León, and G. Platero, Merging of dirac points and floquet topological transitions in ac-driven graphene, Phys. Rev. B **88**, 245422 (2013).

[41] Y. T. Katan and D. Podolsky, Modulated Floquet Topological Insulators, Phys. Rev. Lett. **110**, 016802 (2013).

[42] G. Usaj, P. M. Perez-Piskunow, L. E. F. Foa Torres, and C. A. Balseiro, Irradiated graphene as a tunable floquet topological insulator, Phys. Rev. B **90**, 115423 (2014).

[43] H. Dehghani, T. Oka, and A. Mitra, Out-of-equilibrium electrons and the hall conductance of a floquet topological insulator, Phys. Rev. B **91**, 155422 (2015).

[44] L. D'Alessio and M. Rigol, Dynamical preparation of floquet chern insulators, Nat. Commun. **6**, 8336 (2015).

[45] T.-S. Xiong, J. Gong, and J.-H. An, Towards large-chern-number topological phases by periodic quenching, Phys. Rev. B **93**, 184306 (2016).

[46] M. S. Rudner, N. H. Lindner, E. Berg, and M. Levin, Anomalous Edge States and the Bulk-Edge Correspondence for Periodically Driven Two-Dimensional Systems, Phys. Rev. X **3**, 031005 (2013).

[47] P. Titum, N, H. Lindner, M. C. Rechtsman, and G. Refael, Disorder-Induced Floquet Topological Insulators, Phys. Rev. Lett. **114**, 056801 (2015).

[48] P. Titum, E. Berg, M. S. Rudner, G. Refael, and N. H. Lindner, Anomalous Floquet-Anderson Insulator as a Nonadiabatic Quantized Charge Pump, Phys. Rev. X **6**, 021013 (2016).

[49] V. Khemani, A. Lazarides, R. Moessner, and S. L. Sondhi, Phase Structure of Driven Quantum Systems, Phys. Rev. Lett. **116**, 250401 (2016).

[50] G. J. Sreejith, A. Lazarides, and R. Moessner, Parafermion chain with $2\pi/k$ Floquet edge modes, Phys. Rev. B **94**, 045127 (2016).

[51] S. Roy and G. J. Sreejith, Disordered chern insulator with a two step floquet drive, Phys. Rev. B **94**, 214203 (2016).

[52] Y. H. Wang, H. Steinberg, P. Jarillo-Herrero, and N. Gedik, Observation of floquet-bloch states on the surface of a topological insulator, Science **342**, 453 (2013).

[53] F. Mahmood, C.-K. Chan, Z. Alpichshev, D. Gardner, Y. Lee, P. A. Lee, and N. Gedik, Selective scattering between floquet-bloch and volkov states in a topological insulator, Nat. Phys. **12**, 306 (2016).

[54] R. Wang, B. Wang, R. Shen, L. Sheng, and D. Y. Xing, Floquet Weyl semimetal induced by off-resonant light, Europhys. Lett. **105**, 17004 (2014).

[55] S. Ebihara, K. Fukushima, and T. Oka, Chiral pumping effect induced by rotating electric fields, Phys. Rev. B **93**, 155107 (2016).

[56] C.-K. Chan, P. A. Lee, K. S. Burch, J. H. Han, and Y. Ran, When Chiral Photons Meet Chiral Fermions: Photoinduced Anomalous Hall Effects in Weyl Semimetals, Phys. Rev. Lett. **116**, 026805 (2016).

[57] H. Hübener, M. A. Sentef, U. de Giovannini, A. F. Kemper, and A. Rubio, Creating stable Floquet-Weyl semimetals by laser-driving of 3D Dirac materials, Nat. Commun. **8**, 13940 (2017).

[58] Z. Yan and Z. Wang, Tunable Weyl Points in Periodically Driven Nodal Line Semimetals, Phys. Rev. Lett. **117**, 087402 (2016).

[59] X.-X. Zhang, T. T. Ong, and N. Nagaosa, Theory of photoinduced floquet weyl semimetal phases, Phys. Rev. B **94**, 235137 (2016).

[60] S.-Y. Xu, C. Liu, I. Belopolski, S. K. Kushwaha, R. Sankar, J. W. Krizan, T.-R. Chang, C. M. Polley, J. Adell, T. Balasubramanian, K. Miyamoto, N. Alidoust, G. Bian, M. Neupane, H.-T. Jeng, C.-Y. Huang, W.-F. Tsai, T. Okuda, A. Bansil, F. C. Chou, R. J. Cava, H. Lin, and M. Z. Hasan, Lifshitz transition and van hove singularity in a three-dimensional topological dirac semimetal, Phys. Rev. B **92**, 075115 (2015).

[61] Z. K. Liu, J. Jiang, B. Zhou, Z. J. Wang, Y. Zhang, H. M. Weng, D. Prabhakaran, S. K. Mo, H. Peng, P. Dudin *et al.*, A stable three-dimensional topological dirac semimetal Cd_3As_2, Nat. Mater. **13**, 677 (2014).

[62] M. Neupane, S.-Y. Xu, N. Alidoust, R. Sankar, I. Belopolski, D. S. Sanchez, G. Bian, C. Liu, T.-R. Chang, H.-T. Jeng, B. Wang, G. Chang, H. Lin, A. Bansil, F. Chou, and M. Z. Hasan, Surface versus bulk dirac state tuning in a three-dimensional topological dirac semimetal, Phys. Rev. B **91**, 241114(R) (2015).

[63] M. Neupane, S.-Y. Xu, R. Sankar, N. Alidoust, G. Bian, C. Liu, I. Belopolski, T.-R. Chang, H.-T. Jeng, H. Lin *et al.*, Observation of a three-dimensional topological dirac semimetal phase in high-mobility Cd_3As_2, Nat. Commun. **5**, 3786 (2014).

[64] T. Liang, Q. Gibson, M. N. Ali, M. Liu, R. J. Cava, and N. P. Ong, Ultrahigh mobility and giant magnetoresistance in the dirac semimetal Cd_3As_2, Nat. Mater. **14**, 280 (2014).

[65] H. Sambe, Steady states and quasienergies of a quantum-mechanical system in an oscillating field, Phys. Rev. A **7**, 2203 (1973).

[66] J. H. Shirley, Solution of the schrödinger equation with a hamiltonian periodic in time, Phys. Rev. **138**, B979 (1965).

[67] M. Grifoni and P. Hänggi, Driven quantum tunneling, Phys. Rep. **304**, 229 (1998).

[68] S. Blanes, F. Casas, J. A. Oteo, and J. Ros, The magnus expansion and some of its applications, Phys. Rep. **470**, 151 (2009).

[69] E. S. Mananga and T. Charpentier, Introduction of the floquet-magnus expansion in solid-state nuclear magnetic resonance spectroscopy, J. Chem. Phys. **135**, 044109 (2011).

[70] K. Hashimoto, S. Kinoshita, K. Murata, and T. Oka, Holographic floquet states: (I) a strongly coupled weyl semimetal, arXiv:1611.03702.

[71] I. Hubac and S. Wilson, On the use of brillouin-wigner perturbation theory for many-body systems, J. Phys. B: At., Mol. Opt. Phys. **33**, 365 (2000).

[72] R. C. Young, L. C. Biedenharn, and E. Feenberg, Continued fraction approximants to the brillouin-wigner perturbation series, Phys. Rev. **106**, 1151 (1957).

[73] T. Mikami, S. Kitamura, K. Yasuda, N. Tsuji, T. Oka, and H. Aoki, Brillouin-Wigner theory for high-frequency expansion in periodically driven systems: Application to Floquet topological insulators, Phys. Rev. B **93**, 144307 (2016).

[74] A. Eckardt, Atomic quantum gases in periodically driven optical lattices, Rev. Mod. Phys. **89**, 011004 (2017).

[75] P. M. Perez-Piskunow, L. E. F. Foa Torres, and G. Usaj, Hierarchy of floquet gaps and edge states for driven honeycomb lattices, Phys. Rev. A **91**, 043625 (2015).

[76] See Supplementary Material at http://link.aps.org/supplemental/10.1103/PhysRevB.96.041126 for the derivation of the low-energy effective Hamiltonians for the Weyl points generated out of the Floquet replicas $n = \pm 1$ near $k_z = \Omega$.

[77] J. A. Ashraff and R. B. Stinchcombe, Exact decimation approach to the green's functions of the fibonacci-chain quasicrystal, Phys. Rev. B **37**, 5723 (1988).

[78] G. Grosso and G. P. Parravicini, *Solid State Physics* (Academic Press, 2014).

[79] M. A. Sentef, M. Claassen, A. F. Kemper, B. Moritz, T. Oka, J. K. Freericks, and T. P. Devereaux, Theory of floquet band formation and local pseudospin textures in pump-probe photoemission of graphene, Nat. Commun. **6**, 7047 (2015).